

Quantum Recurrent Unit: A Parameter-Efficient Quantum Neural Network Architecture for NISQ Devices

Tzong-Daw Wu ¹ and Hsi-Sheng Goan ^{1,2,3,*}

¹*Department of Physics and Center for Theoretical Physics, National Taiwan University, Taipei 106319, Taiwan*

²*Center for Quantum Science and Engineering, National Taiwan University, Taipei 106319, Taiwan*

³*Physics Division, National Center for Theoretical Sciences, Taipei 106319, Taiwan*

* Email: goan@phys.ntu.edu.tw

Abstract

The rapid growth of modern machine learning models presents fundamental challenges in parameter efficiency and computational resource requirements. This study introduces the Quantum Recurrent Unit (QRU), a novel quantum neural network architecture specifically designed to address these challenges while remaining compatible with Noisy Intermediate-Scale Quantum (NISQ) devices. QRU leverages quantum controlled-SWAP (C-SWAP, or Fredkin) gates to implement an information selection mechanism inspired by classical Gated Recurrent Units (GRUs), enabling selective processing of temporal information via quantum operations. Through its innovative recurrent architecture featuring measurement results feedforward state propagation and shared parameters across time steps, QRU achieves constant circuit depth and constant parameter count regardless of input sequence length, effectively circumventing the stringent hardware constraints of NISQ computers. We systematically validate QRU's performance through three progressive experiments: oscillatory behavior prediction tasks, high-dimensional feature classification of the Wisconsin Diagnostic Breast Cancer (WDBC) dataset, and MNIST handwritten digit classification. QRU uses only 72 parameters to match a 197-parameter GRU in time series prediction, 35 parameters to achieve 96.13% accuracy equivalent to a 167-parameter Artificial Neural Network (ANN) in WDBC classification, and 132 parameters to reach 98.05% accuracy, outperforming a Convolutional Neural Network (CNN) using approximately 27,265 parameters in MNIST handwritten digit classification. These results demonstrate that QRU consistently achieves comparable or superior performance with significantly fewer parameters than classical neural networks, while maintaining constant quantum circuit depth regardless of input sequence length. The architecture's quantum-native design, combining C-SWAP-based information selection with novel recurrent processing, suggests QRU's potential as a fundamental building block for next-generation machine learning systems,

offering a promising pathway toward more efficient and scalable quantum machine learning architectures compatible with near-term quantum hardware.

Keywords: Quantum Machine Learning, Parameter Efficiency, NISQ, Quantum Neural Networks, Recurrent Neural Networks

1. Introduction

Modern machine learning development faces a fundamental challenge: As task complexity increases, model sizes continue to expand. Neural networks, serving as the foundational building blocks for Transformers, Convolutional Neural Networks (CNNs), and various types of Recurrent Neural Networks (RNNs), exhibit significant parameter growth as input dimensions increase [1]. This growth not only imposes substantial computational and memory complexity but also limits the model's application in resource-constrained scenarios. In particular, within current complex machine learning architectures, the parameter efficiency of neural network components has become a critical factor constraining further development.

Quantum computing, as an emerging computational paradigm, offers new possibilities for addressing this fundamental challenge. By leveraging quantum mechanical properties such as superposition, entanglement and interference, quantum systems demonstrate unique computational advantages: they can not only process large amounts of data simultaneously and achieve acceleration in various complex problems [2-5], but more importantly, they exhibit excellent parameter efficiency [6,7], capable of implementing complex function mappings with fewer adjustable parameters [8,9]. Furthermore, quantum computing may potentially lead to lower energy consumption [10,11], offering new insights into addressing the resource efficiency challenges faced by modern machine learning. These advantages of quantum systems collectively point to a possibility: replacing classical neural networks with parameterized quantum circuits to achieve fundamental breakthroughs in parameter efficiency.

However, in the current Noisy Intermediate-Scale Quantum (NISQ) [12] era, translating quantum advantages into practical machine-learning performance remains a significant challenge. Quantum computers are limited by finite quantum capacity [13] and are susceptible to decoherence and noise. While existing quantum machine learning research [14-17] has demonstrated advantages in specific scenarios, it often remains constrained by the number of qubits and circuit depth when handling high-dimensional data [18]. How to effectively utilize quantum resources under these practical constraints has become a core issue in quantum machine learning.

The Quantum Recurrent Unit (QRU) proposed in this paper provides an innovative solution to this problem. Our QRU's design goal is to serve as a quantum alternative to classical neural networks, addressing the fundamental challenge of parameter efficiency and the hardware limitations of the NISQ era. Through recurrent architecture design, our QRUs achieve constant circuit depth and constant parameter count regardless of sequence length. As a fundamental building block, could replace

classical neural network components in modern machine learning architectures, significantly reducing parameter requirements while maintaining or improving performance. This architecture implements efficient information processing through quantum controlled-SWAP (C-SWAP, or Fredkin) gates [19], leveraging both quantum operations and recurrent structure to optimize resource utilization.

Through three representative experiments, we systematically validate QRU's performance and parameter efficiency: first verifying its fundamental capability as a recurrent architecture through oscillatory behavior prediction tasks, then demonstrating its versatility through two challenging applications - high-dimensional feature classification using the Wisconsin Diagnostic Breast Cancer (WDBC) [20] dataset and image classification using MNIST [21] handwritten digits. These experimental results not only confirm QRU's advantages in parameter usage but also suggest its potential as an alternative to neural networks.

2. QRU Model

In this section, we introduce our QRU, a quantum recurrent neural network specifically designed for NISQ architectures. To fully understand QRU's design philosophy, we first review relevant theoretical foundations. Given that QRU's information selection mechanism draws inspiration from the Gated Recurrent Unit (GRU), we review the core concepts of classical GRU, the basic principles of quantum computing, and the universal approximation properties of quantum circuits. We then detail QRU's architectural design, from its overall structure to each key component, including its recurrent processing mechanism.

2.1 Review of Related Theory

2.1.1 Key Aspects of Quantum Computing

Quantum computing leverages quantum state superposition, entanglement, and interference to process information, offering unique computational advantages for specific tasks. As Wu et al. [22] showed, quantum neural networks possess superior expressivity, capable of implementing complex function mappings with relatively few adjustable parameters. However, in the current NISQ era, quantum computers are limited by finite quantum capacity, necessitating careful consideration of qubit-count and circuit-depth constraints when designing quantum algorithms. These hardware limitations are a primary consideration in our QRU design.

2.1.2 Update and Reset Mechanisms in Classical GRU

GRU [23] is an efficient variant of recurrent neural networks, with its core idea centered on controlling information propagation through update gates and reset gates. As illustrated in Figure 2.1, the GRU architecture processes sequential information through three key components: the reset gate, the update gate, and the generation of the candidate hidden state. The reset gate r_t and update gate z_t are computed from the current input x_t and previous hidden state h_{t-1} , and then control the generation of candidate hidden state \tilde{h}_t and final hidden state h_t . The

reset gate r_t determines how much of the previous hidden state information to use when computing the candidate hidden state, while the update gate z_t controls the balance between retaining old information and incorporating new information.

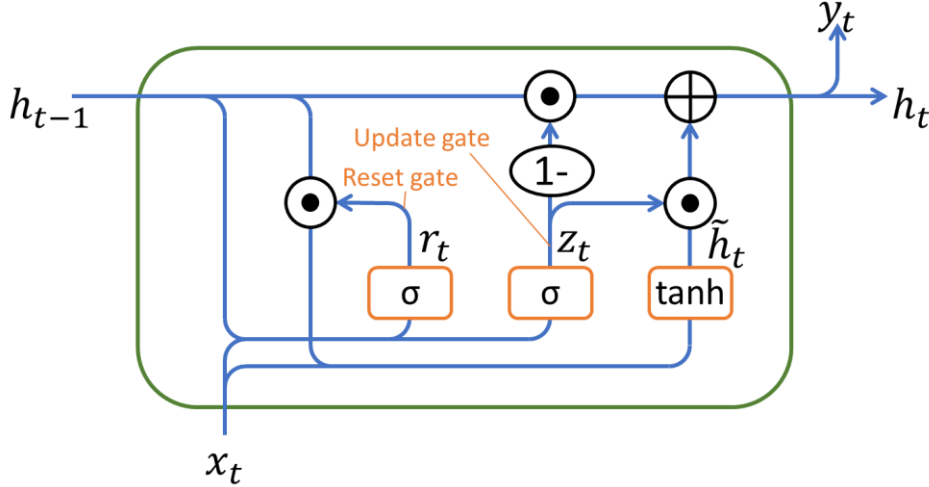


Figure 2.1: Classical Gated Recurrent Unit (GRU) architecture illustrating the computational flow described in equations (1)-(4). The reset gate controls information flow from the previous hidden state h_{t-1} , the update gate determines the mixing ratio between previous and new information, and element-wise operations enable selective information processing, where \odot denotes element-wise multiplication and \oplus denotes addition. This information selection and mixing mechanism inspires QRU's quantum controlled-SWAP operations.

This mechanism can be expressed mathematically as:

$$z_t = \sigma(W_z x_t + U_z h_{t-1} + b_z), \quad (1)$$

$$r_t = \sigma(W_r x_t + U_r h_{t-1} + b_r), \quad (2)$$

$$\tilde{h}_t = \tanh(W_h x_t + U_h (r_t \odot h_{t-1}) + b_h), \quad (3)$$

$$h_t = (1 - z_t) \odot h_{t-1} + z_t \odot \tilde{h}_t, \quad (4)$$

where σ is the sigmoid activation function, \odot represents element-wise multiplication, W and U are trainable weight matrices, and b are bias vectors. Notably, equation (4) embodies GRU's core: using the update gate z_t to dynamically adjust the mixing ratio of old and new information. This adaptive information selection mechanism provides important inspiration for subsequent quantum implementation.

2.1.3 Universal Approximation Properties of Quantum Circuits

A fundamental theoretical result shows that quantum circuits possess universal approximation capability. Pérez-Salinas et al. [9] demonstrated that even parameterized circuits with a single qubit and data-reuploading have universal approximation properties. Schuld et al. [7] further investigated how data encoding strategies affect the expressivity of quantum machine learning models, particularly how appropriate encoding can enhance model expressivity in multi-qubit systems.

These findings provide fundamental theoretical support for the design of quantum neural network architectures, demonstrating the feasibility of implementing neural computations with quantum circuits.

2.1.4 Current Status and Challenges of Quantum Recurrent Models

Recent research in quantum recurrent neural networks has primarily focused on migrating classical architectures to quantum frameworks. For instance, the quantum Long Short-Term Memory (LSTM) proposed by Chen et al. [24] and the quantum GRU architecture developed by Ceschini et al. [25] both replace classical neural network layers with variational quantum circuits (VQC). While intuitive, these approaches maintain classical LSTM/GRU gating logic for temporal processing. The state update rules remain classical operations, limiting full utilization of quantum advantages and adaptability to future fault-tolerant architectures.

Beyond hybrid architectures, fully quantum recurrent approaches have also been explored. Bausch [26] proposed a quantum RNN (QRNN) using parametrized quantum neurons with polynomial activation functions and amplitude amplification, achieving 90.8-98.6% accuracy on MNIST binary digit classification, with approximately 1,200 parameters. While demonstrating the feasibility of QRNNs, the architecture's repeat-until-success circuits and amplitude amplification may limit the scalability for longer sequences. Alternative VQC-based approaches [27, 28] maintain quantum hidden states across time steps, demonstrating compact implementations (e.g., 55 parameters in Takaki's work [28]). However, these approaches implement basic recurrent processing without gating mechanisms analogous to GRU or LSTM, potentially limiting their ability to capture long-term dependencies. Additionally, maintaining quantum coherence throughout sequences requires extremely high-fidelity gates to prevent error accumulation across sequential operations, and extended coherence times to preserve quantum information—both pose practical limitations for NISQ devices.

These limitations have prompted us to reconsider the design approach for quantum recurrent architectures, particularly how to build an architecture that fully leverages quantum advantages through task-specific mechanisms inspired by classical GRU while maintaining NISQ compatibility.

2.2 QRU Architecture Design

2.2.1 Architecture Overview

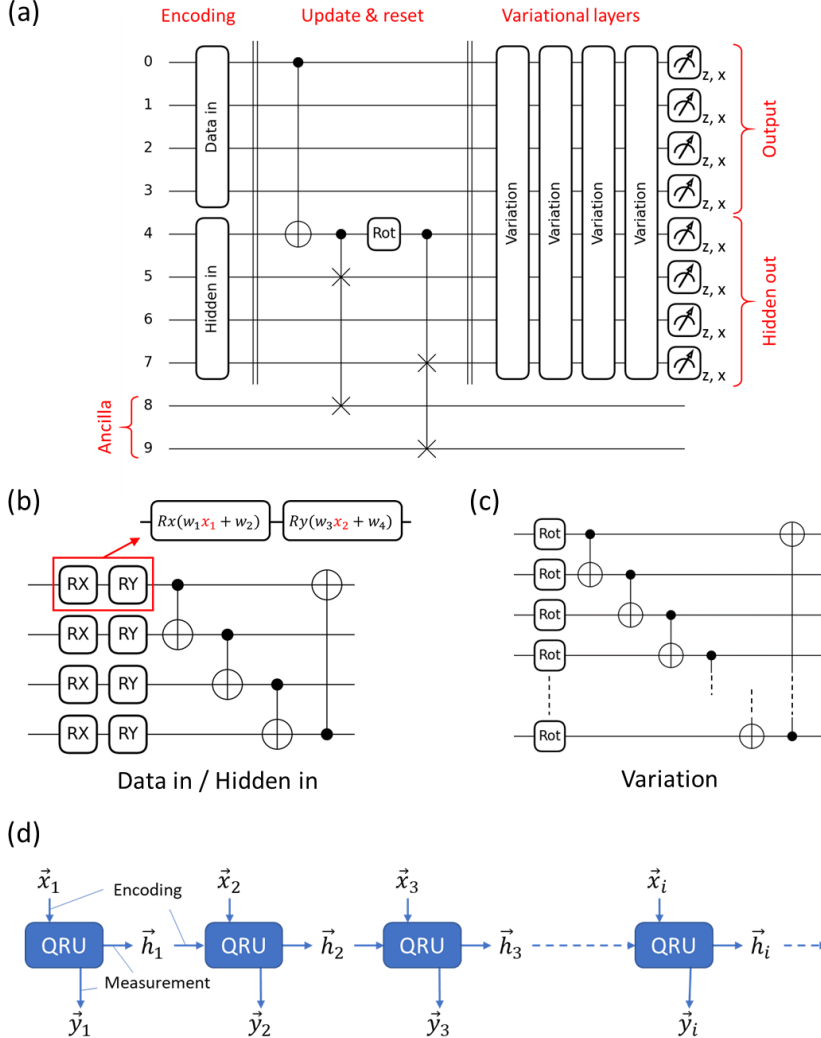


Figure 2.2: QRU Architecture Diagram. (a) Shows a representative QRU circuit architecture with 4 data qubits, 4 hidden qubits, and 2 ancilla qubits, demonstrating the four main components: input and hidden state encoding, update and reset mechanism, variational layers, and output generation through quantum measurements. Data qubits provide computational outputs, while hidden qubits enable the propagation of temporal information to the next time step. (b) Details the structure of the encoding circuit, showing how rotation gates and entangling CNOT gates are used for input and hidden state encoding. (c) Illustrates the combination pattern of rotation (Rot) gates and entangling CNOT gates in the variational layer. (d) Shows the recurrent processing structure in which multiple QRUs process sequential data, with hidden states propagated between time steps through measurement results feedforward schemes to enable modeling of temporal dependencies.

Figure 2.2 illustrates QRU's architectural design, which includes four main components and their recurrent processing structure:

- **Input and Hidden State Encoding:** Converting classical data into rotation angles for quantum states using angle encoding schemes. (Section 2.2.2)

- Update and Reset Mechanism: Using quantum controlled-SWAP (C-SWAP) operations to mimic classical GRU's update and reset logic through selective information processing. (Section 2.2.3)
- Variational Layers: Composed of parameterized quantum gates for approximating complex functions. (Section 2.2.4)
- Output and Hidden State Update: Producing model outputs and updating hidden states through quantum measurements in Z and X bases. (Section 2.2.5)
- Recurrent Processing Structure: Connecting multiple QRUs to process sequential data with a measurement results feedforward scheme [29,30], enabling state propagation and temporal dependency modeling with a constant quantum circuit depth regardless of sequence length. (Section 2.2.6)

2.2.2 Input and Hidden State Encoding

In the encoding phase, as shown in Figure 2.2(b), QRU adopts an efficient angle encoding scheme for both input data and hidden states. This encoding converts values (x_1, x_2) into rotation angles for gates:

$$\begin{aligned} R_x(\theta_1) &= R_x(w_1 x_1 + w_2), \\ R_y(\theta_2) &= R_y(w_3 x_2 + w_4), \end{aligned} \quad (5)$$

where w_1, w_2, w_3, w_4 are trainable parameters. Each qubit can encode two dimensions of information through R_x and R_y gates, and quantum entanglement is introduced through circular CNOT entanglement topology, implementing correlations between qubits. This design fully utilizes the state space of qubits while maintaining a moderate depth in the encoding circuit.

2.2.3 Update and Reset Mechanism

QRU implements an information selection mechanism similar to GRU using quantum controlled-SWAP (C-SWAP) or Fredkin gates [31]. As discussed in Section 2.1.2 regarding the GRU update mechanism, the QRU also needs to balance retaining information from the previous hidden state and incorporating new information.

As shown in Figure 2.3, a C-SWAP operation allows the system to selectively swap the states of two target qubits based on the state of the control qubit:

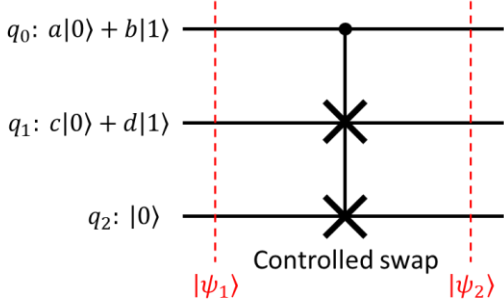


Figure 2.3: Update and Reset Mechanism Diagram of QRU, showing how C-SWAP operations achieve selective state exchange to accomplish information-selective updates.

This quantum mechanism can be described by state evolution:

$$\begin{aligned}
 |\psi_1\rangle &= ac|000\rangle + ad|010\rangle + bc|100\rangle + bd|110\rangle \\
 &\downarrow \\
 |\psi_2\rangle &= ac|000\rangle + ad|010\rangle + bc|100\rangle + bd|101\rangle.
 \end{aligned} \tag{6}$$

The corresponding expectation value of the Pauli-Z operator on qubit q1 evolves as:

$$\begin{aligned}
 \langle\psi_1|\sigma_z(q_1)|\psi_1\rangle &= c^2 - d^2 \\
 &\downarrow \\
 \langle\psi_2|\sigma_z(q_1)|\psi_2\rangle &= a^2(c^2 - d^2) + b^2,
 \end{aligned} \tag{7}$$

where $\sigma_z(q_1)$ represents the Pauli-Z operator acting on qubit q1. This evolution process implements GRU's update mechanism through quantum operations in a more integrated way. The control qubit q_0 , through coefficients a^2 and b^2 , not only determines the mixing ratio but also participates in introducing new information during the quantum evolution. The target qubit q_1 undergoes state changes through the C-SWAP operation, corresponding to the hidden state transformation. The ancilla qubit q_2 enables this selective state exchange, making the controlled information update possible.

In QRU's implementation, information selection operates at two levels: the C-SWAP operation itself provides fine-grained mixing control through quantum amplitudes, while the selective application to specific qubits enables coarse-grained architectural control. Not all qubits participate in C-SWAP operations; some undergo controlled swaps, while others retain their information unchanged, mimicking GRU's selective update behavior, in which different hidden state elements experience different degrees of modification.

This quantum-native approach leverages the properties of quantum superposition states to simultaneously achieve information update and fusion, unlike GRU's sequential process of first generating candidate states and then mixing them with previous states.

2.2.4 Variational Layers

The design of variational layers, as shown in Figure 2.2(c), builds upon the theoretical basis of quantum circuits' approximation properties discussed in Section 2.1.3. Each layer contains multiple rotation gates with independent trainable parameters, serving as the primary information processing component after the QRU's update mechanism. While quantum circuits theoretically possess universal approximation capability, our design focuses on achieving practical processing power under NISQ device constraints through its circuit structure.

2.2.5 Output and Hidden State Update

After processing through variational layers, each qubit is measured in the Z and X bases at the end of each QRU. The measurement results for all qubits are split into two parts, serving two crucial purposes: generating output for the current time step and updating hidden states to feed forward to the next QRU. While the output provides the model's prediction or classification results, the hidden states fed forward to the following QRU play a key role in maintaining temporal information processed by QRU's update mechanism, which is elegantly implemented through C-SWAP operations, providing an information foundation for the next time step's processing. By performing measurements in different bases, we can obtain richer information from quantum states, thereby ensuring effective transmission of information across the time dimension.

2.2.6 Recurrent Processing Structure

As shown in Figure 2.2(d), multiple QRUs are connected in sequence through a measurement results feedforward scheme to process sequential data, forming a recurrent architecture. Each QRU processes input data \vec{x}_i and receives hidden states \vec{h}_i from the previous time step, generating both output vectors \vec{y}_i and updated hidden states for subsequent processing. At the end of each QRU, quantum measurements are performed on each of the qubits. The measurement results are categorized into two parts: one as system output and the other as hidden states fed forward to the next QRU.

The use of a measurement results feedforward scheme between quantum circuits has been explored for constructing quantum NN architectures. Lai [29] demonstrated this approach for depth scaling, employing classical activation-like nonlinearity between the measurement and re-encoding with independent parameters per layer. While the QRU model adopts a similar measurement-and-re-encoding connection pattern, it applies this to temporal processing with shared parameters across time steps, enabling recurrent computation and parameter efficiency.

Specifically, the hidden state propagation follows a specific encoding process: hidden qubits are measured in both the Z and X bases to extract expectation values, which are then fed forward and encoded into the next QRU using the same angle encoding scheme shown in Figure 2.2(b). This ensures that temporal information processed by the current QRU's update mechanism is effectively transmitted to subsequent processing steps.

Through this design, the QRU model's architecture with measurement results feedforward and shared parameters across different QRUs ensures that both the effective quantum circuit depth and the total parameter count remain constant, determined solely by a single QRU, regardless of sequence length. This enables the processing of arbitrary-length sequences while maintaining NISQ compatibility.

Beyond scalability in sequence length, this architecture addresses another key challenge in quantum machine learning: enabling the QRU model to handle arbitrary input and output dimensions via sequential processing. This dimensional flexibility makes the model adaptable to diverse task requirements while operating within NISQ device constraints.

3. Experimental Validation

3.1 Experimental Design Overview

This study validates QRU's performance and universality through three progressive experiments. The first experiment focuses on time series prediction, selecting oscillatory behavior prediction as basic validation, which is not only a typical application of RNNs but also an ideal test scenario for evaluating QRU's temporal modeling capabilities. The second experiment extends to high-dimensional feature processing, using the WDBC dataset classification task to validate QRU's effectiveness in handling high-dimensional data. The third experiment further extends to the image recognition domain, using MNIST handwritten digit recognition tasks to demonstrate QRU's performance in handling more complex visual data.

All experiments use the PennyLane [32] quantum machine learning framework combined with JAX [33] backend. Although these experiments simulate quantum circuits on classical computers, we take fundamental quantum computing properties and resources into consideration in the design, such as qubit count usage and circuit depth control. The choice of the simulation environment is primarily due to the extensive iterative training requirements of machine learning, where each model training run involves thousands of iterations, making the implementation on current real quantum computers, with limited availability and access times, expensive and impractical for such intensive computational demands.

While these three experiments differ in application scenarios, they adopt similar training strategy frameworks. For optimization, all experiments use the Adam optimizer and implement dynamic learning rate adjustment mechanisms. Specifically, the system records training loss values at fixed intervals (10 or 100 epochs, depending on experimental settings). When observing that three consecutive recorded loss values are all higher than the fourth-last recording, the system automatically halves the learning rate and reverts to the model parameter state with the lowest loss value during that training period to continue training. This adaptive mechanism effectively prevents training instability issues caused by excessive learning rates, ensuring robust model convergence to optimal solutions.

To prevent overfitting, each experiment employs an early stopping mechanism, with stopping conditions adjusted to different task characteristics and data structures. Similarly, the choice of loss functions varies based on task objectives.

Regarding model architecture, the QRU structures in all three experiments are based on the basic architecture described in Section 2 but differ in specific implementation details to optimize the performance-efficiency balance for each task. The hidden-state configurations range from 4 to 5 qubits, each measured in both the Z and X bases to extract expectation values (yielding 8- to 10-dimensional hidden-state representations), and the variational layer designs range from single-parameter to three-parameter rotation gates across 3 to 4 measurement-result feedforward circuit layers. These configurations were determined through preliminary experiments to achieve stable performance while maintaining parameter efficiency for the specific task complexity. The detailed specifications for each experiment are presented in the respective experimental sections.

With these flexible configurations, we adopt a progressive validation strategy. Although QRU's ultimate goal is to serve as a quantum alternative to classical neural networks, as a first step, we need to validate its basic capability as a recurrent architecture. Therefore, in time series prediction tasks, we compare against GRU and LSTM, as these mature classical RNN models provide good benchmarks. After confirming QRU's recurrent processing capabilities, we further validate its performance on more challenging tasks: high-dimensional feature classification (WDBC) and visual data processing (MNIST), demonstrating QRU's potential as a universal neural network alternative. This progressive experimental design allows us to systematically evaluate QRU's spectrum from basic capabilities to universal applications.

3.2 Oscillatory Behavior Prediction: Basic Temporal Capability Validation

3.2.1 Experimental Method

The first experiment aims to validate QRU's basic capabilities for modeling and predicting time-series data. By simultaneously handling Simple Harmonic Oscillation and Damped Oscillation with a single model, we evaluate the model's adaptability and generalization ability to different oscillation patterns. In particular, the introduced self-feedback prediction mechanism further demonstrates the model's potential in handling long-term temporal dependencies.

The experiment uses two sets of time-series data, each containing 150 data points, comprising sequences of simple harmonic oscillation and damped oscillation. The first 100 data points from each dataset are used for joint training of the model, while the remaining 50 points serve as the test set to evaluate the model's predictive performance. During training, a step-by-step prediction approach is adopted, in which the model receives a single data point as input and predicts the value for the next time step, learning to handle both oscillation patterns simultaneously.

Given that this task involves one-dimensional time-series data, we implement a QRU with 5 hidden qubits and 4-layer variational circuits—a configuration determined through preliminary experiments following the approach outlined in Section 3.1. Specifically, the QRU uses a single qubit with a single Rx rotation gate for data encoding; the hidden state is implemented using 5 qubits to realize a 10-dimensional state representation; the variational layers are constructed from 4 layers of quantum circuits, each utilizing $U2(\varphi, \lambda)$ rotation gates—two-parameter single-qubit rotations implementing $Rz(\varphi)Ry(\pi/2)Rz(\lambda)$ —with φ and λ as trainable parameters. These layers then generate prediction output by measuring the Z-basis expectation value of the first qubit. The overall architecture contains 72 trainable parameters. The complete circuit architecture is shown in Supplementary Figure S1.

Model training uses Mean Squared Error (MSE) as the loss function. To demonstrate the model's generalization ability, a joint training strategy is adopted, enabling the same model to learn the dynamic characteristics of both simple harmonic oscillation and damped oscillation simultaneously. To prevent overfitting, an early stopping mechanism is implemented, terminating training when the decrease in training loss recorded every 100 epochs is less than 1% for three consecutive recordings.

For comprehensive statistical analysis, we conducted 50 independent experiments for different parameter configurations of each model type. Specifically, QRU uses a fixed configuration of 72 parameters, classical GRU tests multiple configurations ranging from 11 to 441 parameters, and LSTM experiments with different scales ranging from 101 to 491 parameters. Each configuration independently executes 50 training runs, each using the same model structure and training strategy but with different parameter initializations. This experimental design, with a systematic parameter sweep, allows us to comprehensively analyze the impact of parameter scale on model performance.

3.2.2 Results Analysis and Comparison

As shown in the detailed statistical metrics in Table 3.1, QRU demonstrates exemplary performance in handling both oscillation patterns across 50 independent experiments. During the training phase, the model achieved a mean MSE of 2.14E-04 with a standard deviation of 2.06E-04, indicating stable learning of both patterns. The original mean MSE in the testing phase was 1.94E-02, which improved to 2.49E-03 after outlier removal, with the standard deviation decreasing from 4.22E-02 to 3.06E-03, indicating stable prediction capabilities of the model.

Table 3.1: QRU Model Performance Statistics in Training and Testing Phases (Including Original Data and Results After Outlier Removal)

	Train	Train (w/o outlier)	Test	Test (w/o outlier)
Mean	2.14E-04	1.65E-04	1.94E-02	2.49E-03
Median	1.64E-04	1.55E-04	1.78E-03	9.67E-04
Std. dev.	2.06E-04	7.84E-05	4.22E-02	3.06E-03

The prediction capability is illustrated in Figure 3.1, which presents a representative experimental result. In the simple harmonic oscillation prediction task (Figure 3.1(a)), the QRU accurately captured the periodicity and amplitude characteristics of the oscillation, with the prediction curve (green line) closely matching the test data (red triangles), indicating that the model successfully learned the fundamental properties of harmonic motion. In the damped oscillation prediction task (Figure 3.1(b)), the model performed equally well, accurately predicting not only the oscillation frequency but also successfully simulating the amplitude decay trend. Notably, even in later prediction periods, the model's output remains consistent with the actual data.

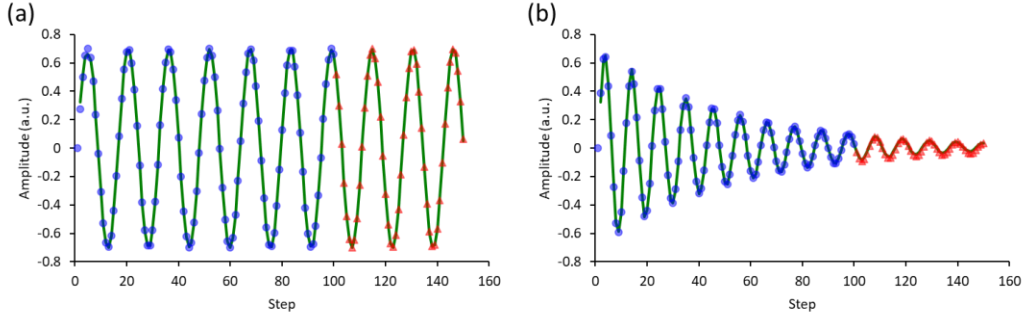


Figure 3.1: Comparison of model predictions with actual data. (a) Simple harmonic oscillation and (b) damped oscillation prediction results, where blue dots represent training data, red triangles represent test data, and the green line represents model predictions.

To evaluate the parameter efficiency of QRU, we first compared it with classical models using similar parameter counts. As shown in Table 3.2, with 72 parameters, QRU (MSE: 2.49E-03) shows substantial improvement in test MSE over both GRU (77 parameters, MSE: 1.05E-01) and LSTM (101 parameters, MSE: 2.14E-01). Moreover, QRU's test standard deviation (4.22E-02) is also smaller than GRU (2.13E-01) and LSTM (1.41E+00), indicating that its predictions are not only more accurate but also more stable.

Table 3.2: Training and Testing MSE Statistics for Three Models with Similar Parameter Counts

	QRU (72)	GRU (77)	LSTM (101)
Train Mean	2.14E-04	2.58E-03	6.08E-05
Train (w/o outlier)	1.65E-04	4.31E-05	6.08E-05
Test Mean	1.94E-02	1.60E-01	7.19E-01
Test (w/o outlier)	2.49E-03	1.05E-01	2.14E-01
Test Std. dev.	4.22E-02	2.13E-01	1.41E+00

Given QRU's superior performance with minimal parameters, we conducted parameter-expansion experiments on classical models to determine how many parameters they would need to achieve comparable performance levels. The results summarized in Table 3.3 show that GRU requires expansion to 197 parameters to

achieve performance levels close to the 72-parameter QRU (MSE: 2.22E-03), while LSTM, even expanded to 491 parameters, still cannot surpass QRU's performance. This significant parameter requirement is further illustrated in Figures 3.2 and 3.3. As shown in Figure 3.2, during the training phase, classical models exhibit performance improvements with increasing parameter counts, though the improvement margin gradually diminishes. The testing phase results in Figure 3.3 further confirm that GRU and LSTM require significantly more parameters to approach QRU's performance level.

Table 3.3: Performance Statistics Comparison of Three Models After Parameter Expansion

	QRU (72)	GRU (197)	LSTM (491)
Train Mean	2.14E-04	3.43E-04	3.42E-05
Train (w/o outlier)	1.65E-04	3.37E-05	3.34E-05
Test Mean	1.94E-02	7.28E-02	4.69E-01
Test (w/o outlier)	2.49E-03	2.22E-03	1.64E-01
Test Std. dev.	4.22E-02	3.85E-01	1.04E+00

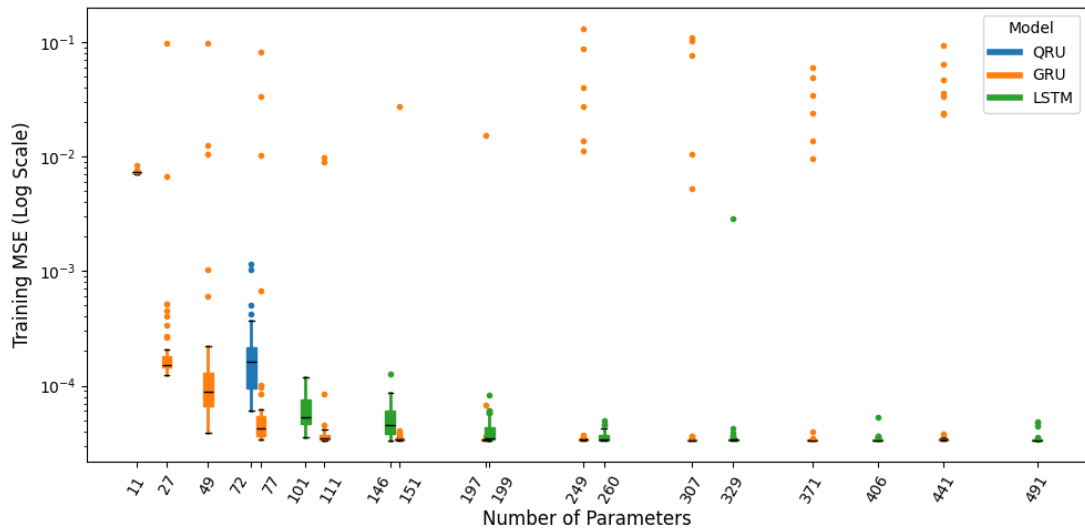


Figure 3.2: Training performance comparison of three models under different parameter scales. Box plots show the MSE distributions for QRU (blue), GRU (orange), and LSTM (green), with 50 independent training runs for each parameter configuration. The X-axis shows the number of model parameters, and the Y-axis shows the corresponding MSE values (in log scale). Each box plot represents the statistical distribution from these training runs.

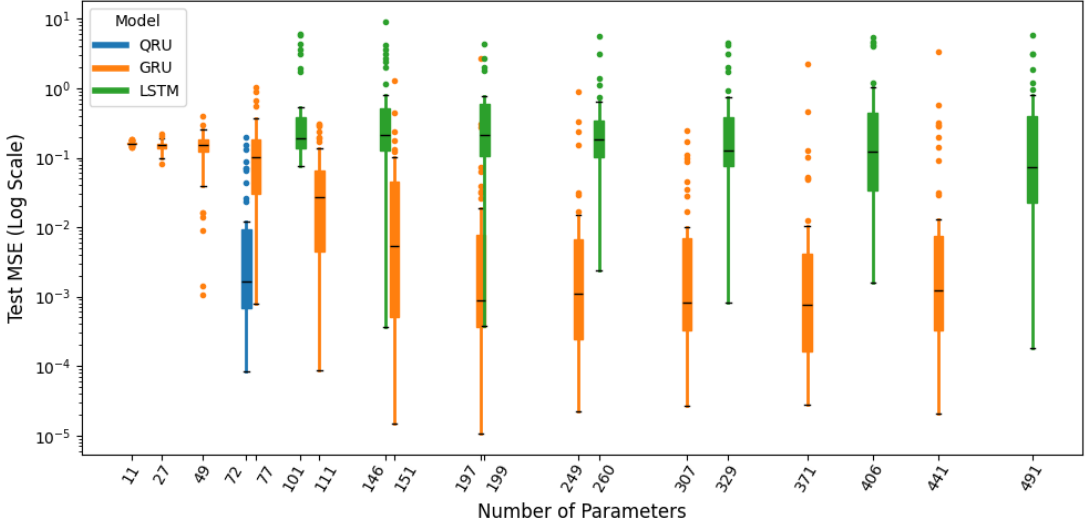


Figure 3.3: Model performance distribution on the test set. Using the same visualization approach as in Figure 3.2, the MSE distributions of three models are shown during the testing phase. Each box plot represents the distribution of test results from 50 independent training runs for a specific parameter configuration, clearly showing the impact of different configurations on model generalization.

3.3 WDBC Classification: High-Dimensional Feature Processing Capability Validation

3.3.1 Experimental Method

This experiment aims to validate QRU's capability in handling high-dimensional feature classification problems. We conduct experiments using the WDBC dataset from the UCI Machine Learning Repository [34]. The dataset contains 30 features extracted from digital images of breast tumor cell nuclei, used to distinguish between benign and malignant tumors.

The dataset comprises 569 samples, including 357 benign tumors and 212 malignant tumors. Given the relatively small dataset, we adopt the Leave-One-Out Cross-Validation (LOOCV) strategy for experimental evaluation to make full use of the limited data. In the data preprocessing phase, we standardize all features, adjusting their ranges to the $[0,1]$ interval. During actual processing, the model sequentially processes these 30 standardized feature values.

The model architecture adopts a sequential processing strategy similar to the oscillation prediction experiment, treating the 30-dimensional features as a one-dimensional sequence of length 30. For this classification task, we implement a QRU with 4 hidden qubits and 3-layer alternating rotation gates, consistent with the configuration approach discussed in Section 3.1. Specifically, the input encoding uses a single qubit with an Rx rotation gate for feature encoding; the hidden state uses 4 qubits to implement an 8-dimensional state representation; the variational layers are constructed with three layers of rotation gates, adopting an alternating design pattern: the first layer uses Rx gates, the second layer uses Ry gates, and the third layer uses

Rx gates again, with each rotation gate containing 1 trainable parameter. The model's final output takes the Z-basis expectation value of the first qubit, and we map the output range from $[-1, +1]$ to $[-s, +s]$ through a trainable parameter s to optimize binary classification effects. The overall model contains 35 trainable parameters. Detailed implementation is provided in Supplementary Figure S2.

The training process employs batch training with a batch size of 20. Since this task focuses on binary classification of tumors into benign and malignant, we use binary cross-entropy as the loss function:

$$loss = -\frac{1}{N} \sum_i^N (y_i \cdot \log(\hat{y}_i) + (1 - y_i) \cdot \log(1 - \hat{y}_i)) \quad (8)$$

where y_i is the true label for the i -th sample (0 for benign, 1 for malignant), \hat{y}_i is the model's predicted probability of the i -th sample being malignant, and N is the number of samples.

To prevent overfitting, we implemented an early stopping mechanism. The system records training loss every 10 epochs, and when the decrease in loss values for three consecutive recordings is less than 1%, the training process is terminated. This design helps stop training when model performance stabilizes, avoiding overfitting to training data.

3.3.2 Results Analysis and Comparison

As shown in Table 3.4, the QRU model shows strong performance on the WDBC classification task. In 569 LOOCV experiments, the model achieved a test accuracy of 96.13%, with a stable training process (training accuracy 97.97%, standard deviation 0.95%). The confusion matrix shows that 347 out of 357 benign samples were correctly identified, and 200 out of 212 malignant samples were correctly identified, with only 10 false positives and 12 false negatives. These results demonstrate that QRU can not only handle time-series prediction problems but also process high-dimensional feature classification tasks effectively, showing its potential as an alternative to classical neural networks.

Table 3.4: Detailed Performance of QRU Model on WDBC Classification Task

Metric Type	Metric	Value
Classification Performance	Test Accuracy	96.13% (547/569)
	Training Accuracy	97.97% ($\pm 0.95\%$)
Confusion Matrix	True Positive (TP)	200
	True Negative (TN)	347
	False Positive (FP)	10
	False Negative (FN)	12
Derived Metrics	Sensitivity	94.33%
	Specificity	97.20%
	Precision	95.24%
	F1-Score	94.79%
Training Process	Mean Epochs	658.23 (± 260.81)
	Epoch Range	80 ~ 2040

More importantly, QRU achieves this performance level using only 35 parameters. As shown in Table 3.5, even compared to neural network benchmark results reported in the UCI Machine Learning Repository (accuracy 92.31%, range 87.41%~96.50%), QRU demonstrates consistent performance. Particularly noteworthy: while some studies achieved higher classification performance through feature engineering, we specifically selected neural network baseline results using the original features (without feature selection or extraction) from these studies for comparison. Compared to classical neural networks using more parameters, such as Guo and Nandi's Multilayer Perceptron (MLP) [35] (65-449 parameters[†], 96.21%), Aalaei et al.'s Artificial Neural Network (ANN) [36] (167 parameters[†], 96.50%), and Rani et al.'s Deep Neural Network (DNN) [37] (1,601 parameters[†], 95.32%), QRU achieves comparable performance levels (96.13%) with fewer parameters (35).

Table 3.5: Different Models' Performance on WDBC Test Set

Model	Parameters [†]	Test Accuracy	Additional Metrics
QRU Model (This study)	35	96.13%	Sen: 94.33%, Spec: 97.20%, Prec: 95.24%, F1: 94.79%
MLP [Guo & Nandi][35]	65~449	96.21% ($\pm 1.73\%$)	-
ANN [Aalaei et al.][36]	167	96.50%	Sen: 98.20%, Spec: 96.00%
MLP [Salama et al.][38]	-	96.66%	-
DNN [Rani et al.][37]	1,601	95.32%	Sen: 95.08%, Spec: 95.45%, Prec: 92.06%, F1: 93.54%
NN [UCI][34]	-	92.31% (87.41%~96.50%)	Prec: 91.64% (86.51%~95.97%)

[†]Parameter counts are estimated based on architecture descriptions and figures in the original papers.

Furthermore, QRU shows balanced performance, with sensitivity (94.33%) and specificity (97.20%); the model maintains high performance across both classes of samples. While other models might have slight advantages in specific metrics, they typically require more parameters to achieve similar performance. This efficient parameter utilization, combined with strong performance in high-dimensional feature classification, demonstrates QRU's potential as a building block for complex machine learning models.

3.4 MNIST Digit Classification: Image Data Processing Capability Validation

3.4.1 Experimental Method

This experiment aims to validate QRU's capability in handling high-dimensional image data. Following the benchmark tests in Bowles et al. [39], we specifically focus on the digit recognition task for "3" and "5" using their MNIST dataset. This pair was chosen in [39] because it is among the hardest digits to distinguish, providing a challenging test scenario for model evaluation. Through converting two-dimensional image data into sequential input, this experiment also demonstrates QRU's flexibility in handling non-sequential data.

The experiment uses the 8×8-pixel version of the MNIST dataset provided by [39], in which the original 28×28 MNIST images were resized using bilinear interpolation to preserve spatial correlation structure. The dataset contains 7,141 samples of "3" and

6,313 samples of "5". We employ 7-fold stratified cross-validation for experimental evaluation, ensuring that each fold preserves the original dataset's class proportions. In each fold's training process, we further randomly extract 1/6 of the training data as a validation set, ultimately forming a 5:1:1 split ratio for training, validation, and test sets.

The implemented QRU structure is specifically designed for high-dimensional data processing. For this task, we implement a QRU with 4 hidden qubits and 4-layer Rot-based variational circuits. Specifically, the input encoding uses 4 qubits, capable of processing 8 features per time step; the hidden state similarly uses 4 qubits, providing 8-dimensional state representation capability; the variational layer uses Rot gates—three-parameter single-qubit rotations implementing $Rz(\omega)Ry(\vartheta)Rz(\phi)$ —and employs 4 variational circuit layers. The model takes the Z-basis expectation values of the output of the first two qubits, which are scaled from $[-1,+1]$ to $[-s,+s]$ via a trainable parameter s to enhance discriminative ability, and then processes them with a softmax function to generate probability distributions for cross-entropy classification. QRU portion of this architecture includes 131 trainable parameters, and together with the scaling parameter s , the overall model has 132 trainable parameters. The full circuit design is presented in Supplementary Figure S3.

In the data preprocessing phase, we first standardize all pixel values, adjusting their range to $[0,1]$. Given QRU's sequential processing nature, we treat each 8×8 image as a sequence of length 8 with a feature dimension of 8. Specifically, each time step inputs one row of pixel data from the image, completing the processing of the entire image over 8 time steps.

The training process uses batch training with a batch size of 50. Although this experiment only uses the "3" and "5" digit classes, to maintain consistency with complete MNIST classification problems, we use cross-entropy rather than binary cross-entropy as the loss function:

$$loss = -\frac{1}{N} \sum_i^N \sum_j^C y_{ij} \log(\hat{y}_{ij}), \quad (9)$$

where y_{ij} is the true label for the i -th sample in the j -th class (one-hot representation, taking values 0 or 1), \hat{y}_{ij} is the model's predicted probability for the i -th sample in the j -th class, N is the number of samples, and C is the number of classes.

To prevent overfitting, an early stopping mechanism is implemented that records the validation set loss every 10 epochs. When no significant change is observed in 10 consecutive recorded validation losses (i.e., the last 9 loss values are not lower than the tenth-last loss value), or the loss value stabilizes with no further change, the training process is terminated.

3.4.2 Results Analysis and Comparison

In the MNIST digit recognition task for "3" and "5", the QRU model demonstrates stable, consistent performance. As shown in Table 3.6, in 7-fold stratified cross-

validation, the QRU model achieved a mean training accuracy of 98.70% (standard deviation 0.30%) and a mean test accuracy of 98.05% (standard deviation 0.42%). Each fold maintained high performance, with training accuracy ranging from 98.17% to 99.11% and test accuracy ranging from 97.61% to 98.75%, demonstrating the model's stability in handling visual data.

Table 3.6: QRU Model Performance in 7-fold Cross-validation

	Training Accuracy	Testing Accuracy	Epochs
Fold-1	98.67%	97.76%	410
Fold-2	98.17%	97.76%	970
Fold-3	98.88%	98.75%	810
Fold-4	98.91%	98.39%	740
Fold-5	98.60%	97.87%	690
Fold-6	98.56%	98.23%	440
Fold-7	99.11%	97.61%	840
Mean	98.70%	98.05%	700

Using only 132 parameters, QRU achieves 98.05% test accuracy on this task. In comparison, the benchmark testing by Bowles et al. [39] showed that a classical CNN required approximately 27,265 parameters to achieve 96.42% accuracy†. The same study also included comparison with two quantum models: Quanvolutional Neural Network (Quanvolutional NN) [40] achieved 91.41% accuracy†, while Wei Net [41] achieved 70.49%†. As shown in Table 3.7, QRU reduces parameter count by 99.5% compared to CNN while achieving higher accuracy. This benchmark test result is particularly valuable as it provides a direct comparison of classical models and different quantum approaches under the same conditions.

Table 3.7: Performance Comparison of Different Methods on MNIST "3" and "5" Classification

Model	Parameters	Training Accuracy Mean (std)	Testing Accuracy Mean (std)
QRU Model (This study)	132	98.70% (±0.30%)	98.05% (±0.42%)
CNN [39]	27,265†	96.79% (±0.79%)	96.42% (±0.64%)†
Quanvolutional NN [39,40]	-	93.24% (±1.10%)	91.41% (±0.91%)†
Wei Net [39,41]	-	70.46% (±0.25%)	70.49% (±0.25%)†

†Parameter counts are estimated from source code, while accuracy values are from the authors' public results.

The performance differences with quantum models in [39] may reflect fundamental design distinctions. Bowles et al. observed that Quanvolutional NN's basis encoding degraded data quality through random feature mapping. Additionally, amplitude-encoding models (including WeiNet) consistently underperformed in their benchmarks, leading the authors to question whether "amplitude embedding [is] just not a good design choice" for their settings.

QRU's angle encoding with trainable scaling parameters and sequential C-SWAP-based information processing offers a contrasting approach that maintains information integrity while enabling adaptive feature selection throughout the temporal pipeline.

These results not only validate QRU's capability in handling high-dimensional visual data but, more importantly, demonstrate its potential as an alternative to classical neural networks. Through maintaining competitive performance while keeping a low parameter count, QRU demonstrates its advantages as a fundamental building block for complex machine learning models.

4. Comprehensive Analysis and Discussion

4.1 Efficiency Analysis

This study systematically validates QRU's efficiency advantages in parameter usage and quantum resource allocation through three different types of experiments. Table 4.1 summarizes the parameter usage and performance comparison between QRU and other models across different task types.

Table 4.1: Cross-task Parameter Efficiency Comparison

Task Type	Model	Parameters	Test Performance	Parameter Overhead†
Time Series Prediction	QRU	72	MSE: 2.49E-03	Baseline
	GRU(77)	77	MSE: 1.05E-01	+6.9%
	GRU(197)	197	MSE: 2.22E-03	+173.6%
	LSTM	491	MSE: 1.64E-01	+581.9%
WDBC Classification	QRU	35	ACC: 96.13%	Baseline
	MLP [35]	65-449	ACC: 96.21%	+634.3% *
	ANN [36]	167	ACC: 96.50%	+377.1%
	DNN [37]	1,601	ACC: 95.32%	+4,474.3%
MNIST Recognition	QRU	132	ACC: 98.05%	Baseline
	CNN [39]	27,265	ACC: 96.42%	+20,547.7%

†Parameter Overhead: Percentage increase in parameters compared to baseline QRU, calculated as $((\text{Model Parameters} - \text{QRU Parameters}) / \text{QRU Parameters}) \times 100\%$

*Calculated using the median of the MLP parameter range

QRU demonstrates remarkable parameter efficiency advantages. In time-series prediction tasks, a 72-parameter QRU achieves performance comparable to that of a 197-parameter GRU. In WDBC classification tasks, QRU using only 35 parameters achieves 96.13% test accuracy, comparable to ANN requiring 167 parameters (96.50%) and DNN requiring 1,601 parameters (95.32%). In MNIST digit recognition tasks, QRU demonstrates high parameter efficiency, achieving higher accuracy (98.05%) with 132 parameters compared to CNN's 96.42% accuracy using 27,265 parameters. Figure 4.1 shows the performance comparison of various models relative to QRU, where performance metrics have been normalized to ratios relative to QRU: for classification tasks, the ratio of model accuracy to QRU accuracy; for time-series prediction tasks, the ratio of QRU's MSE to the model's MSE.

The significant reduction in parameter count demonstrated in our experiments can be attributed to QRU's architectural efficiency. While classical GRU architecture requires separate neural networks with substantial parameters for each component (update

gate, reset gate, and candidate generation), QRU achieves similar functionality through quantum-native operations—specifically, using C-SWAP gates for information selection, which eliminates the need for multiple parameter-heavy networks.

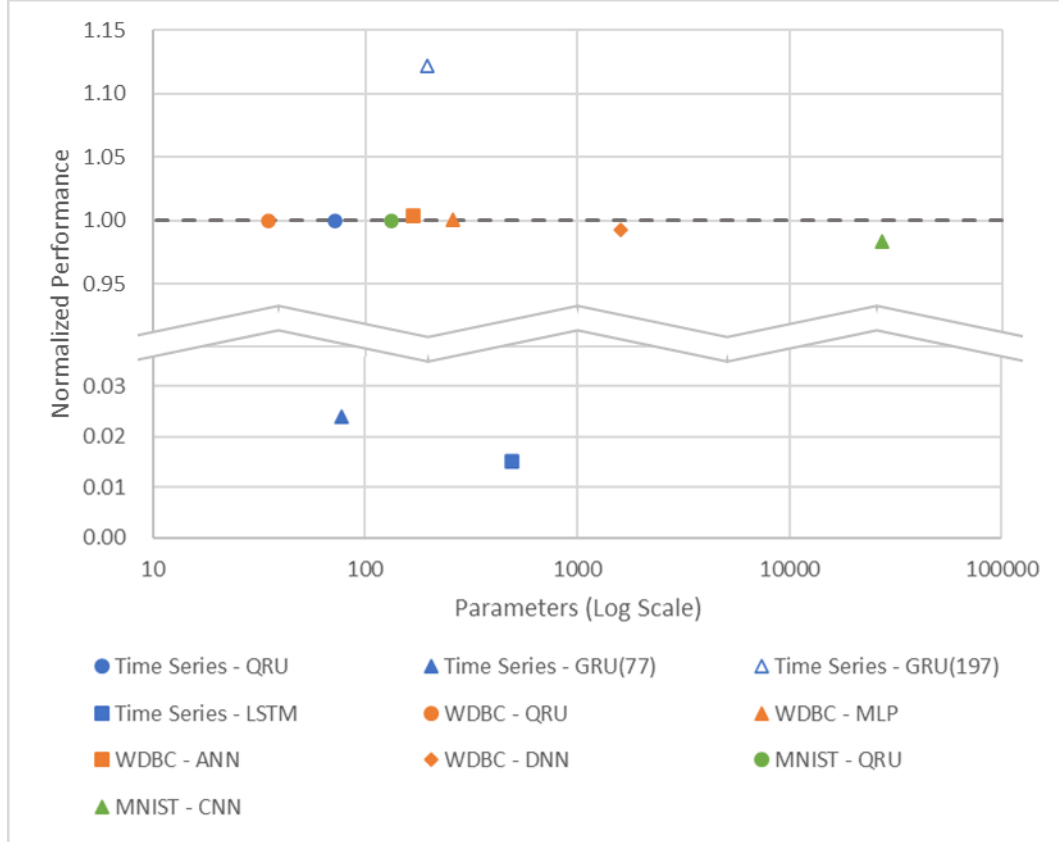


Figure 4.1 Parameter-performance comparison across different tasks. All performance metrics are normalized relative to QRU (set as 1.0). For classification tasks (WDBC and MNIST), the metric represents the ratio of model accuracy to QRU accuracy. For time-series prediction, the metric is the ratio of QRU's MSE to the model's MSE. The X-axis shows the number of parameters on a log scale. The break in the Y-axis accommodates the full range of normalized performance while maintaining resolution in the region of interest.

Moreover, QRU's efficient parameter scaling is maintained regardless of input dimension, as demonstrated in our experiments across different tasks. This consistent efficiency makes QRU particularly attractive for large-scale applications where parameter efficiency is critical. While other quantum approaches might achieve similar parameter reductions, they often require deeper circuits or multiple VQCs, therefore limiting their practicality in NISQ devices [24, 40-44].

Regarding quantum resource allocation, QRU achieves unique efficiency through its recurrent structure. This design allows sequential processing of high-dimensional input features through limited qubits while effectively retaining and integrating key information. Across the three experiments, QRU used 8, 7, and 10 qubits, respectively, including input, hidden state, and ancilla qubits. This stable quantum resource usage, combined with the structured variational circuit design, demonstrates QRU's practical

efficiency under NISQ constraints, where both qubit count and circuit depth are critical considerations. Importantly, each QRU terminates with quantum measurements and feeds the measurement results forward to the next time step, ensuring that the total quantum circuit depth remains effectively confined within a single QRU regardless of sequence length, thereby mitigating the stringent circuit-depth constraints of NISQ devices.

4.2 Model Characteristics Analysis

Through three progressive experiments, we observe several key characteristics of QRU that demonstrate its potential beyond parameter efficiency. These characteristics stem from the integration of recurrent structure and C-SWAP operations as well as the measurement results feedforward scheme, showing how these quantum-native mechanisms can be effectively utilized for neural network design under NISQ constraints.

Unlike standard VQC approaches that often require fixed input-output dimensions, QRU's recurrent structure enables processing of arbitrary-dimensional data in a sequential manner. Our experiments across different domains - from time-series prediction to image classification - validate this flexibility, demonstrating that the architecture can effectively handle diverse data types and tasks.

The information update mechanism in QRU leverages quantum-native C-SWAP operations, representing an approach distinct from classical neural network design principles. Rather than relying on parametric transformations to select and mix previous and present information, QRU implements this information selection mechanism via C-SWAP operations (see Section 2.2.3). This design demonstrates how such quantum operations enable efficient neural information processing, particularly in implementing state update and reset operations with minimal quantum resources.

The integration of quantum information selection and recurrent processing with the measurement results feedforward scheme demonstrates QRU's potential as a building block for modern machine learning architectures. This design approach suggests new possibilities for developing quantum neural network components that are both versatile and hardware-aware, particularly valuable in the NISQ era. The success of this implementation opens the door to integration into various machine learning architectures, providing a practical template for future quantum machine learning designs.

4.3 Limitations and Future Prospects

Building upon QRU's demonstrated advantages, future research should focus on establishing a comprehensive theoretical foundation and addressing practical challenges. Key areas include analyzing mechanisms of quantum state evolution and their impact on efficiency, exploring scaling and integration options with existing architectures, and investigating implementation challenges on physical quantum devices, from noise mitigation to performance optimization. Specifically, future research could include:

1. Establishing a theoretical framework for quantum state evolution in QRU, deeply analyzing theoretically the contribution of hybrid quantum-classical properties to parameter efficiency.
2. Exploring QRU's integration feasibility in larger machine learning architectures (such as Transformers).
3. Studying QRU's performance and scalability in large-scale problems.
4. Validating QRU's advantages on physical quantum computers, particularly its performance when facing more complex problems.
5. Exploring quantum state preservation by bypassing hidden state measurements, enabling direct quantum state propagation between units without re-encoding overhead for future fault-tolerant quantum computers.

5. Conclusion

The QRU model presented in this study represents a significant step toward realizing practical quantum neural networks that can operate effectively within the constraints of current NISQ-era quantum hardware. By carefully designing quantum circuits that respect hardware constraints while leveraging quantum-native operations for efficient information processing, we have created an architecture that achieves remarkable parameter efficiency across diverse applications. Through three different types of experiments, we systematically validated QRU's performance and universality: from basic time-series prediction to high-dimensional feature classification in medical diagnosis, and finally to visual data recognition. Across all experimental tasks, QRU achieves comparable or superior performance while consistently requiring fewer parameters than classical approaches.

QRU's success validates the approach of building quantum machine learning systems from the ground up, using quantum operations to implement neural network functionality rather than simply translating classical architectures into quantum circuits. The controlled-SWAP-based information selection mechanism, measurement results feedforward recurrent processing, and shared parameters across time steps enable efficient parameter utilization while maintaining the essential temporal processing capabilities of recurrent networks and provide a template for developing other quantum neural network components.

As quantum hardware continues to improve with increasing qubit counts, longer coherence times, and higher gate fidelities, architectures like QRU will become increasingly practical and powerful. The principles demonstrated here, quantum-native design, NISQ compatibility, parameter efficiency, and architectural versatility, point toward a future where QRUs serve as fundamental building blocks in advanced machine learning systems.

Ultimately, this work contributes to the ongoing effort to harness quantum mechanical properties for practical computational advantages. By demonstrating that QRUs can match or exceed classical neural network performance with dramatically

fewer parameters while achieving constant quantum circuit depth regardless of input sequence length, we provide evidence that quantum machine learning is not merely a theoretical possibility but an emerging reality with significant potential for transforming how we approach artificial intelligence and machine learning in the quantum era.

Acknowledgements

H.-S. Goan acknowledges support from the National Science and Technology Council (NSTC), Taiwan, under Grants No. NSTC 113-2112-M-002-022-MY3, No. NSTC 113-2119-M-002-021, No. 114-2119-M-002-018, No. NSTC 114-2119-M-002-017-MY3, from the US Air Force Office of Scientific Research under Award Number FA2386-23-1-4052 and from the National Taiwan University under Grants No. NTU-CC-115L8937, No. NTU-CC115L893704 and No. NTU-CC-115L8512. H.-S. Goan. is also grateful for the support of the “Center for Advanced Computing and Imaging in Biomedicine (NTU-115L900702)” through the Featured Areas Research Center Program within the framework of the Higher Education Sprout Project by the Ministry of Education (MOE), Taiwan, the support of Taiwan Semiconductor Research Institute (TSRI) through the Joint Developed Project (JDP) and the support from the Physics Division, National Center for Theoretical Sciences, Taiwan.

References

- [1] Goodfellow, I., Bengio, Y., & Courville, A. (2016). Deep learning. MIT Press.
- [2] Childs, A. M., & van Dam, W. (2010). Quantum algorithms for algebraic problems. *Reviews of Modern Physics*, 82(1), 1-52. <https://doi.org/10.1103/RevModPhys.82.1>
- [3] Abrams, D. S., & Lloyd, S. (1999). Quantum algorithm providing exponential speed increase for finding eigenvalues and eigenvectors. *Physical Review Letters*, 83(24), 5162-5165. <https://doi.org/10.1103/PhysRevLett.83.5162>
- [4] Shor, P. W. (2001). Introduction to quantum algorithms. arXiv. <https://doi.org/10.48550/arXiv.quant-ph/0005003>
- [5] Trivedi, L. M., Elumalai, M., Reddy, N. S., Prasad, A. K., Jose, B. K., & Patra, J. P. (2023). Quantum computing algorithms for solving complex mathematical problems. *International Journal on Recent and Innovation Trends in Computing and Communication*, 11(10), 2202-2206. <https://doi.org/10.17762/ijritcc.v11i10.8913>
- [6] Huang, H. Y., Broughton, M., Mohseni, M., Babbush, R., Boixo, S., Neven, H., & McClean, J. R. (2021). Power of data in quantum machine learning. *Nature Communications*, 12(1). <https://doi.org/10.1038/s41467-021-22539-9>
- [7] Schuld, M., & Killoran, N. (2019). Quantum machine learning in feature Hilbert spaces. *Physical Review Letters*, 122(4), 040504. <https://doi.org/10.1103/PhysRevLett.122.040504>

[8] Tangpanitanon, J., Thanasilp, S., Dangniam, N., Lemonde, M. A., & Angelakis, D. G. (2020). Expressibility and trainability of parametrized analog quantum systems for machine learning applications. *Physical Review Research*, 2(4). <https://doi.org/10.1103/physrevresearch.2.043364>

[9] Pérez-Salinas, A., López-Núñez, D., García-Sáez, A., Forn-Díaz, P., & Latorre, J. I. (2021). One qubit as a universal approximant. *Physical Review A*, 104(1). <https://doi.org/10.1103/physreva.104.012405>

[10] Abegaz, B. W., Mahajan, S. M., & Johnson, R. W. (2015). Power consumption analysis of computing facilities with superconducting Josephson junction quantum computers. In 2015 IEEE 15th International Conference on Environment and Electrical Engineering (EEEIC) (pp. 1351-1356). IEEE. <https://doi.org/10.1109/EEEIC.2015.7165366>

[11] Meier, F., & Yamasaki, H. (2023). Energy-consumption advantage of quantum computation. *arXiv*. <https://doi.org/10.48550/arXiv.2305.11212>

[12] Preskill, J. (2018). Quantum computing in the NISQ era and beyond. *Quantum*, 2, 79. <https://doi.org/10.22331/q-2018-08-06-79>

[13] Cross, A. W., Bishop, L. S., Sheldon, S., Nation, P. D., & Gambetta, J. M. (2019). Validating quantum computers using randomized model circuits. *Physical Review A*, 100(3). <https://doi.org/10.1103/physreva.100.032328>

[14] Biamonte, J., Wittek, P., Pancotti, N., Rebentrost, P., Wiebe, N., & Lloyd, S. (2017). Quantum machine learning. *Nature*, 549(7671), 195-202. <https://doi.org/10.1038/nature23474>

[15] Mishra, N., Kapoor, A., Sharma, T., & Mondal, H. S. (2021). Quantum machine learning: A review and current status. In N. Sharma, A. Chakrabarti, V. E. Balas, & J. Martinovic (Eds.), *Data management, analytics and innovation* (pp. 75-87). Springer. https://doi.org/10.1007/978-981-15-5619-7_8

[16] Havlíček, V., Córcoles, A. D., Temme, K., Harrow, A. W., Kandala, A., Chow, J. M., & Gambetta, J. M. (2019). Supervised learning with quantum-enhanced feature spaces. *Nature*, 567(7747), 209-212. <https://doi.org/10.1038/s41586-019-0980-2>

[17] Schuld, M., Sønke, R., & Meyer, J. J. (2021). Effect of data encoding on the expressive power of variational quantum-machine-learning models. *Physical Review A*, 103(3). <https://doi.org/10.1103/physreva.103.032430>

[18] Cerezo, M., Verdon, G., Huang, H. Y., Cincio, L., & Coles, P. J. (2022). Challenges and opportunities in quantum machine learning. *Nature Computational Science*, 2, 567-576. <https://doi.org/10.1038/s43588-022-00311-3>

[19] Fredkin, E., & Toffoli, T. (2002). Conservative logic. In A. Adamatzky (Ed.), *Collision-based computing*. Springer. https://doi.org/10.1007/978-1-4471-0129-1_3

[20] Wolberg, W. H., Street, W. N., & Mangasarian, O. L. (1995). Computer-derived nuclear features distinguish malignant from benign breast cytology. *Human Pathology*, 26(7), 792-796. [https://doi.org/10.1016/0046-8177\(95\)90229-5](https://doi.org/10.1016/0046-8177(95)90229-5)

[21] LeCun, Y., Bottou, L., Bengio, Y., & Haffner, P. (1998). Gradient-based learning applied to document recognition. *Proceedings of the IEEE*, 86(11), 2278-2324. <https://doi.org/10.1109/5.726791>

[22] Wu, Y., Yao, J., Zhang, P., & Zhai, H. (2021). Expressivity of quantum neural networks. *Physical Review Research*, 3(3). <https://doi.org/10.1103/physrevresearch.3.l032049>

[23] Cho, K., van Merriënboer, B., Gulcehre, C., Bahdanau, D., Bougares, F., Schwenk, H., & Bengio, Y. (2014). Learning phrase representations using RNN encoder-decoder for statistical machine translation. *arXiv*. <https://doi.org/10.48550/arXiv.1406.1078>

[24] Chen, S. Y. C., Yoo, S., & Fang, Y. L. L. (2022). Quantum long short-term memory. In 2022 IEEE International Conference on Acoustics, Speech and Signal Processing (ICASSP) (pp. 8622-8626). IEEE. <https://doi.org/10.1109/ICASSP43922.2022.9747369>

[25] Ceschini, A., Rosato, A., & Panella, M. (2024). A variational approach to quantum gated recurrent units. *Journal of Physics Communications*, 8(8), 085004. <https://doi.org/10.1088/2399-6528/ad6db7>

[26] Bausch, J. (2020). Recurrent quantum neural networks. In H. Larochelle, M. Ranzato, R. Hadsell, M. F. Balcan, & H. Lin (Eds.), *Advances in Neural Information Processing Systems* (Vol. 33, pp. 1368-1379). Curran Associates, Inc.

[27] Li, Y., Wang, Z., Han, R., Shi, S., Li, J., Shang, R., Zheng, H., Zhong, G., & Gu, Y. (2023). Quantum recurrent neural networks for sequential learning. *Neural Networks*, 166, 148-161. <https://doi.org/10.1016/j.neunet.2023.07.003>

[28] Takaki, Y., Mitarai, K., Negoro, M., Fujii, K., & Kitagawa, M. (2021). Learning temporal data with a variational quantum recurrent neural network. *Physical Review A*, 103(5), 052414. <https://doi.org/10.1103/PhysRevA.103.052414>

[29] Lai, H.-W. (2020). Deep neural network with quantum circuits and hybrid neurons [Master's thesis, National Taiwan University]. National Taiwan University Repository. <https://doi.org/10.6342/NTU202003988>

[30] Tacchino, F., Barkoutsos, P., Macchiavello, C., Tavernelli, I., Gerace, D., & Bajoni, D. (2020). Quantum implementation of an artificial feed-forward neural network. *Quantum Science and Technology*, 5(4), 044010. <https://doi.org/10.1088/2058-9565/abb8e4>

[31] Fredkin, E., & Toffoli, T. (1982). Conservative logic. *International Journal of Theoretical Physics*, 21(3–4), 219–253. <https://doi.org/10.1007/BF01857727>

[32] Bergholm, V., Izaac, J., Schuld, M., Gogolin, C., Terilla, J., & Killoran, N. (2018). PennyLane: Automatic differentiation of hybrid quantum-classical computations. *arXiv*. <https://doi.org/10.48550/arXiv.1811.04968>

[33] Bradbury, J., Frostig, R., Hawkins, P., Johnson, M. J., Leary, C., Maclaurin, D., & Wanderman-Milne, S. (2018). JAX: Composable transformations of Python+NumPy programs [Computer software]. <http://github.com/google/jax>

[34] Wolberg, W., Mangasarian, O., Street, N., & Street, W. (1993). Breast Cancer Wisconsin (Diagnostic) [Dataset]. UCI Machine Learning Repository. <https://doi.org/10.24432/C5DW2B>

[35] Guo, H., & Nandi, A. K. (2006). Breast cancer diagnosis using genetic programming generated feature. *Pattern Recognition*, 39(5), 980-987. <https://doi.org/10.1016/j.patcog.2005.10.001>

[36] Aalaei, S., Shahraki, H., Rowhanimanesh, A., & Eslami, S. (2016). Feature selection using genetic algorithm for breast cancer diagnosis. *Iranian Journal of Basic Medical Sciences*, 19(5), 476-482. PMID: 27403253; PMCID: PMC4923467.

[37] Rani, P., Kumar, R., & Ahmed, O. S. (2023). PCA-DNN: A novel deep neural network oriented system for breast cancer classification. *EAI Transactions on Pervasive Health Technology*. <https://doi.org/10.4108/eetpht.9.3533>

[38] Salama, G. I., Abdelhalim, M. B., & Zeid, M. A. (2012). Experimental comparison of classifiers for breast cancer diagnosis. In 2012 Seventh International Conference on Computer Engineering & Systems (ICCES) (pp. 180-185). <https://doi.org/10.1109/ICCES.2012.6408508>

[39] Bowles, J., Ahmed, S., & Schuld, M. (2024). Better than classical? The subtle art of benchmarking quantum machine learning models. *arXiv:2403.07059*. <https://doi.org/10.48550/arXiv.2403.07059>

[40] Henderson, M., Shakya, S., Pradhan, S., & Cook, T. (2019). Quanvolutional neural networks: Powering image recognition with quantum circuits. *arXiv:1904.04767*. <https://doi.org/10.48550/arXiv.1904.04767>

[41] Wei, S., Chen, Y., Zhou, Z., & Yu, H. (2022). A quantum convolutional neural network on NISQ devices. *AAPPS Bulletin*, 32, 2. <https://doi.org/10.1007/s43673-021-00030-3>

[42] Cong, I., Choi, S., & Lukin, M. D. (2019). Quantum convolutional neural networks. *Nature Physics*, 15, 1273–1278. <https://doi.org/10.1038/s41567-019-0648-8>

[43] Ding, X., Song, Z., Xu, J., Hou, Y., Yang, T., & Shan, Z. (2024). Scalable parameterized quantum circuits classifier. *Scientific Reports*, 14, 15886. <https://doi.org/10.1038/s41598-024-66394-2>

[44] Zhou, L., Fang, L., Xi, R., & Xu, J. (2023). Multi-channel quantum convolutional neural network for image classification. *Quantum Machine Intelligence*, 5, 30. <https://doi.org/10.1007/s42484-023-00130-3>

Supplementary Material: Detailed QRU Implementation

This document provides comprehensive implementation details for the three experimental validations of the Quantum Recurrent Unit (QRU) architecture described in the main text. Each section includes detailed circuit specifications, parameter configurations, and processing methodologies that complement the conceptual framework presented in Section 2 of the main text.

S1. Oscillatory Behavior Prediction Implementation

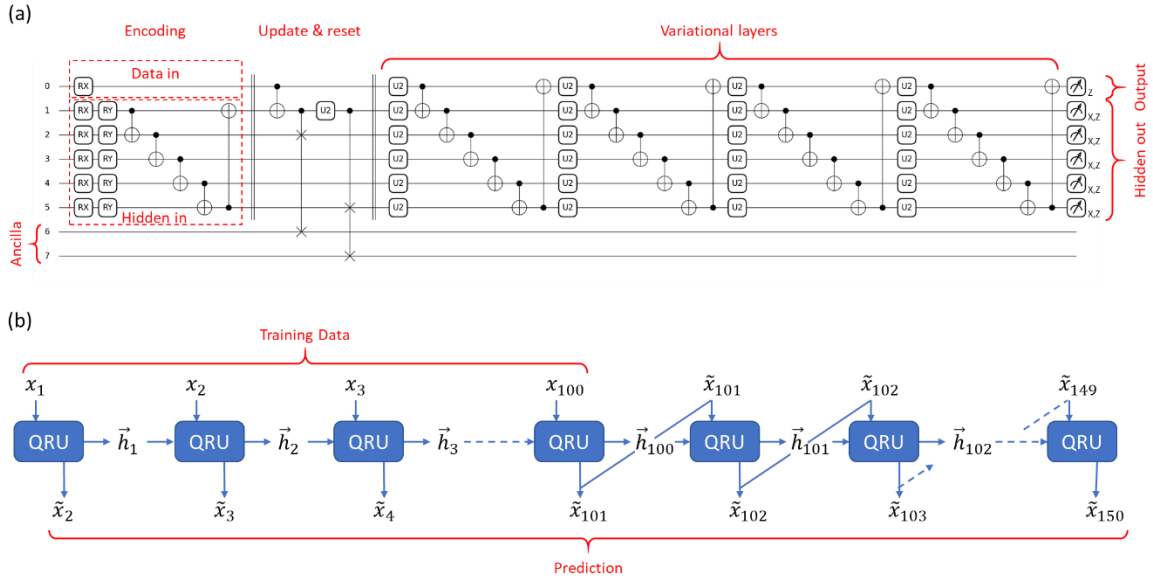


Figure S1: QRU circuit implementation for oscillatory behavior predictions. (a) Circuit architecture with 1 data qubit and 5 hidden qubits. (b) Sequential processing flow showing training and prediction phases.

S1.1 Circuit Architecture

The oscillatory prediction experiment employs a QRU configuration explicitly designed for one-dimensional time series modeling (Figure S1(a)). The circuit uses 1 data qubit (qubit 0) for input encoding and 5 hidden qubits (qubits 1-5) for temporal state representation, providing a 10-dimensional hidden state space through Z and X basis measurements.

Input encoding utilizes a single Rx rotation gate with trainable parameters, suitable for one-dimensional scalar input. The choice of Rx gates provides sufficient expressivity for encoding oscillatory patterns while maintaining circuit simplicity.

Hidden state encoding follows the same angle encoding scheme as described in Figure 2.2(b) of the main text. The 10-dimensional hidden state vector (obtained from measuring 5 qubits in both Z and X bases at the previous time step) is encoded into the 5 hidden qubits using Rx and Ry rotation gates with trainable parameters. Each qubit encodes two dimensions of hidden state information through its Rx and Ry

rotations, with circular CNOT entanglement operations implementing correlations between qubits.

The update & reset mechanism implements controlled-SWAP operations on selected qubits to enable information-selective processing, mimicking the classical GRU's update gate functionality. Not all qubits participate in swap operations, allowing partial retention of information that balances the integration/mixing of old and new information.

Four variational layers form the core computational component, each containing $U2(\varphi, \lambda)$ rotation gates with 2 trainable parameters per gate. $U2$ gates are two-parameter single-qubit rotations implementing $Rz(\varphi)Ry(\pi/2)Rz(\lambda)$, providing rich expressivity for function approximation while maintaining compatibility with NISQ device constraints.

S1.2 Sequential Processing Framework

The experiment processes two types of oscillatory data through the sequential framework shown in Figure S1(b). The processing follows a step-by-step prediction paradigm where the model receives a single scalar input x_i and predicts the next time step value \tilde{x}_{i+1} , with hidden states \vec{h}_i propagated between steps.

The training phase (steps 1-100) uses true data values (x_1-x_{100}) from both oscillation types, enabling the model to learn the underlying dynamics of both patterns simultaneously. This joint training strategy tests the model's capability to distinguish and generalize across different oscillatory behaviors.

The prediction phase ($\tilde{x}_{101}-\tilde{x}_{150}$) implements a self-feedback mechanism where each prediction output becomes the input for the subsequent time step. Specifically, the output \tilde{x}_{101} from step 100 serves as input for step 101, and this pattern continues through step 149, producing final prediction \tilde{x}_{150} . This self-feedback approach evaluates the model's ability to maintain long-term temporal dependencies and generate coherent predictions without external ground truth.

S1.3 Technical Specifications

- Total qubits: 6 (1 data + 5 hidden)
- Total trainable parameters: 72
- Input dimension: 1 (scalar time series values)
- Output dimension: 1 (scalar prediction)
- Hidden state dimension: 10 (5 qubits \times 2 bases)
- Training data: 100 time steps per oscillation type
- Test data: 50 prediction steps with self-feedback

S2. WDBC Classification Implementation

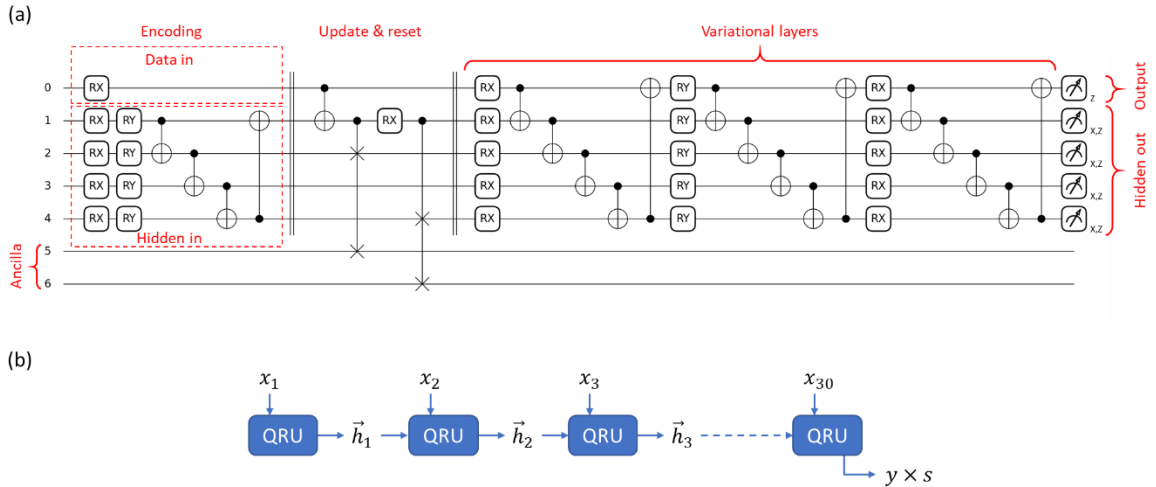


Figure S2: QRU circuit implementation for WDBC classification. (a) Circuit architecture with 1 data qubit and 4 hidden qubits. (b) Sequential processing of 30-dimensional feature vectors.

S2.1 Circuit Architecture

The WDBC classification experiment uses a QRU configuration adapted for high-dimensional feature processing (Figure S2(a)). The circuit employs 1 data qubit for input encoding and 4 hidden qubits for temporal state representation, providing an 8-dimensional hidden state space.

Input and hidden state encoding follow the same angle encoding principles described in S1.1, with Rx and Ry rotation gates processing sequential feature inputs and hidden state propagation.

The architectural difference lies in the variational layers, which consist of 3 layers with alternating Rx-Ry-Rx rotation gates, each gate containing 1 trainable parameter. This alternating gate pattern provides sufficient expressivity for distinguishing between benign and malignant tumor features while maintaining parameter efficiency.

Output generation measures the Z-basis expectation value of the first qubit at the final processing step, with an additional scaling parameter s applied for binary classification optimization.

S2.2 Sequential Processing Framework

The experiment processes the 30-dimensional WDBC feature vector as a sequential input (x_1-x_{30}), treating each feature as a time step in a temporal sequence (Figure S2(b)). This approach allows the QRU model's recurrent architecture to handle high-dimensional data through its inherent sequential processing capability.

Each of the 30 features (extracted from digital images of breast tumor cell nuclei) is fed sequentially into the single data qubit, with the model maintaining temporal dependencies through its hidden state mechanism (\vec{h}_i). The raw output is scaled by a

trainable parameter s ($y \times s$), then processed through a sigmoid function for binary classification optimization. Training uses binary cross-entropy loss for malignant/benign tumor classification.

S2.3 Technical Specifications

- Total qubits: 5 (1 data + 4 hidden)
- Total trainable parameters: 35 (including scaling parameter s)
- Input sequence length: 30 features
- Output dimension: 1 (binary classification score)
- Hidden state dimension: 8 (4 qubits \times 2 bases)
- Evaluation method: Leave-One-Out Cross-Validation (LOOCV)

S3. MNIST Digit Recognition Implementation

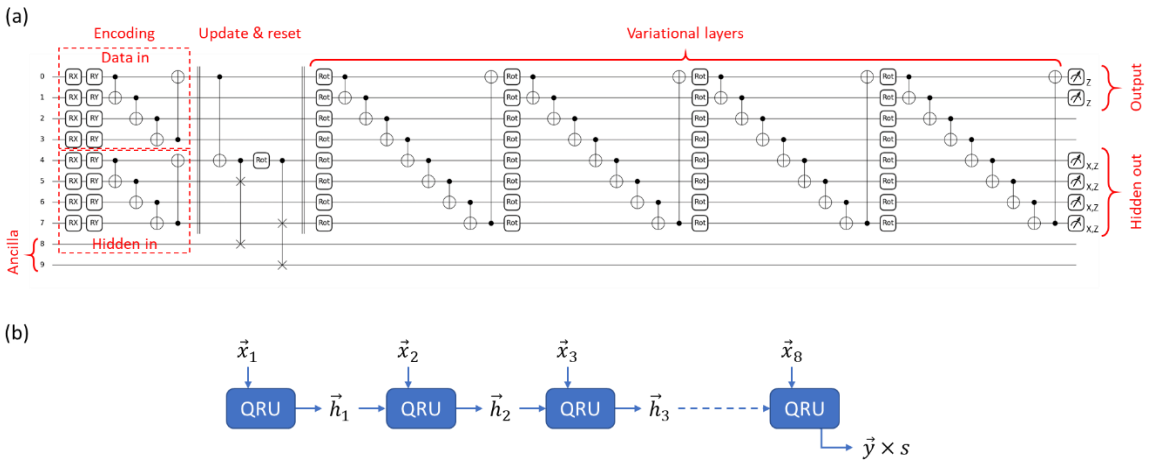


Figure S3: QRU circuit implementation for MNIST digit recognition. (a) Circuit architecture with 4 data qubits and 4 hidden qubits. (b) Sequential processing of 8×8 images over 8 time steps.

S3.1 Circuit Architecture

The MNIST digit recognition experiment demonstrates QRU's capability in processing high-dimensional image data (Figure S3(a)). The circuit uses 4 data qubits for input encoding and 4 hidden qubits for temporal state representation, providing an 8-dimensional hidden state space.

Input and hidden state encoding follow the same angle encoding framework as described in S1.1, with the key difference being the increased data qubit count to handle higher-dimensional input vectors.

The variational layers consist of 4 layers using Rot gates (three-parameter single-qubit rotations implementing $Rz(\omega)Ry(\vartheta)Rz(\phi)$), each containing 3 trainable parameters.

This configuration provides enhanced expressivity suitable for the complexity of image recognition tasks.

Output generation measures the Z-basis expectation values of the first two qubits at the final processing step, creating a 2-dimensional output vector that is scaled by parameter s and processed through softmax for binary classification between digits "3" and "5".

S3.2 Sequential Processing Framework

The experiment processes 8x8 pixel images through a sequential temporal framework (Figure S3(b)). Each 8x8 image is treated as a sequence of 8 time steps ($\vec{x}_1 - \vec{x}_8$), where each time step inputs one row of 8 pixel values. This row-by-row processing approach converts 2D spatial information into 1D temporal sequences, allowing the QRU model's recurrent architecture to handle image data through its natural sequential processing capability.

The 4 data qubits enable processing of 8 features per time step, with each qubit encoding 2 pixel values through Rx and Ry rotations. After 8 time steps, the complete image has been processed sequentially. The 2-dimensional raw output is scaled by a trainable parameter s ($\vec{y} \times s$), then processed through a softmax function to generate probability distributions for the two digit classes ("3" and "5"). Training uses cross-entropy loss for classification optimization.

This sequential image processing demonstrates the QRU model's flexibility in handling non-temporal data by leveraging its recurrent structure to process spatial information through temporal decomposition.

S3.3 Technical Specifications

- Total qubits: 8 (4 data + 4 hidden)
- Total trainable parameters: 132 (including scaling parameter s)
- Input sequence length: 8 time steps
- Input dimension per time step: 8 pixel values
- Output dimension: 2 (binary classification vector)
- Hidden state dimension: 8 (4 qubits \times 2 bases)
- Image size: 8x8 pixels
- Evaluation method: Stratified 7-fold cross-validation